HiLL PUBLISHING

OAJRC Material Science, 2025, 7(1), 13-23
https://www.hillpublisher.com/journals/oajrcms/
ISSN Online: 2632-2072

A Perspective of Recent Progress in Zn_3P_2 (II-V) Diluted Magnetic Semiconductors for Spintronic Applications

Nakka Praveenkumar[1], K. V. Madhuri[1,*], Nasina Madhusudhana Rao[2], Lakshmi Rajesh Chebrolu[3], G Chinna Venkata Subbaiah[4], Anjali Bhattacharyya[2], Anju Babu[2], Ch. Linga Raju[5]

[1]Thin Film Research Center, Department of Physics, Vignan's Foundation for Science, Technology & Research (Deemed to be University), Vadlamudi, Guntur (Dt), Andhra Pradesh 522213, India.
[2]Department of Physics, School of Advanced Sciences, VIT-AP University, Inavolu, Beside AP Secretariat, Amaravati, Andhra Pradesh 522237, India.
[3]MLR Institute of Technology, Hyderabad, Telangana 500043, India.
[4]Department of Physics, Annamacharya University, Rajampet, Andhra Pradesh 516126, India.
[5]Department of Physics, Acharya Nagarjuna University, Nagarjuna Nagar, Andhra Pradesh 522510, India.

How to cite this paper: Nakka Praveenkumar, K. V. Madhuri, Nasina Madhusudhana Rao, Lakshmi Rajesh Chebrolu, G Chinna Venkata Subbaiah, Anjali Bhattacharyya, Anju Babu, Ch. Linga Raju. (2025) A Perspective of Recent Progress in Zn3P2 (II-V) Diluted Magnetic Semiconductors for Spintronic Applications. *OAJRC Material Science*, 7(1), 13-23.
DOI: 10.26855/oajrcms.2025.06.002

Received: August 28, 2025
Accepted: September 25, 2025
Published: October 21, 2025

***Corresponding author:** K. V. Madhuri, Thin Film Research Center, Department of Physics, Vignan's Foundation for Science, Technology & Research (Deemed to be University), Vadlamudi, Guntur (Dt), Andhra Pradesh 522213, India.

Abstract

Recently, the addition of impurities or dopants has significantly altered the properties of Zn_3P_2. Doping has led to enhancements in various applications, including electrical, spintronic, optoelectronic devices, and lithium-ion batteries. Due to its direct band gap energy, luminescence, and room-temperature ferromagnetic behavior, Zn_3P_2 has shown improved performance in different forms such as single crystals, thin films, powders, and nanostructures. This review highlights the current theoretical and experimental understanding of ferromagnetism in Zn_3P_2 and other II-V diluted magnetic semiconductors, with a particular focus on the properties of Zn_3P_2-based diluted magnetic semiconductors. The transition elements influence the host (Zn_3P_2) system and magnetic order at low dopant concentrations. We explained the Zn_3P_2 system's theoretical and experimental studies on how it is influenced by spintronic applications. We talk about the various uses of the Zn_3P_2 system in the future as well as the impacts of magnetic interactions. Moreover, we discussed recent literature on Zn_3P_2 and its results, with the key directions of development, serving as beginning, an orientation, and stimulation for upcoming research.

Keywords

Magnetism; Semiconductors; Spintronic materials; Zn_3P_2 system and II-V alloy

1. Introduction

The discovery of spin-dependent electron transport channels in solid-state devices in the 1960s provided the impetus for the creation of spintronics as a field of research. A recent field called spintronics combines the intrinsic spin property of electrons with charge. Today, dilute magnetic semiconductors (DMSs) are popular for spintronics device materials. The most common DMS materials fall into the II-IV, IV-VI, and II-VI classifications [1]. It is possible to create these diluted magnetic semiconductors by doping host semiconductor material with transition metal and rare earth elements such as Fe, Mn, Ni, Gd, Nd, etc. Diluted magnetic semiconductors require room-temperature ferromagnetism to operate. These days, versatile and sophisticated electronic devices are crucial due to their affordability and mobility. "Spintronics," which was

developed to address this unmet need, is one of the emerging technologies that might be utilized to produce a new class of electronic devices. The ability of large integrated circuits to control electron flow in semiconductor materials offers significant benefits for both processing and communications technologies [2]. High-speed networks require a large number of electronic transistors in an integrated system. Incorporating and positioning a high number of transistors is challenging, and because of their sheer quantity, they use a lot of power and produce more heat. To overcome these limitations in traditional electrical systems, the researchers resorted to spintronics instead of electronics. Magnetism is first incorporated into non-magnetic semiconductors to create spintronic devices [3]. Future electronic gadgets will have to overcome challenges including synthesizing materials with semiconducting and ferromagnetic properties. In spintronics devices, electrons' inherent magnetic moments and spin may be seen and manipulated in addition to their fundamental charge. Dilute magnetic semiconductors are excellent candidates for spintronic devices because they can behave as ferromagnetic semiconductors with a variety of characteristics. Consequently, during the last 20 years, research on DMS materials has exploded. In recent times, the concept of "spintronics" has gained significant attention due to a notable finding in magnetic ion-doped II-VI semiconductor compounds and oxides, that highlights the manifestation of ferromagnetism [4]. This discovery could enable semiconductor devices to harness both electron spin and charge, opening up new possibilities in device design and functionality.

The II-V dilute magnetic semiconductors (DMS) include compounds like Cd_3P_2, $ZnAs_2$, Zn_3As_2, Cd_3As_2, and Zn_3P_2. To be useful, these materials must exhibit ferromagnetism at room temperature when doped with transition metals or rare earth elements. This has mostly been theorized by several researchers. Very limited people reported on Zn_3P_2 material based on experimental studies. One of the class II-V semiconducting materials, zinc phosphide (Zn_3P_2), is a polar, mixed-valent, earth-abundant, and inexpensive semiconducting substance. Zinc phosphide is a p-type semiconducting material that is easily produced as thin films and nanoparticles [5-8]. Zinc phosphide has good photovoltaic potential and a direct band gap of 1.5 eV at 300 K [9]. The P42/nmc space group (No. 137) describes the initial tetragonal structure of the Zn_3P_2 and unit cell of Zn_3P_2, where a = b = 8.0970, and c = 11.4500 and $\alpha = \beta = \gamma = 90°$ [10]. Zn_3P_2 has a high carrier diffusion length and optical absorption coefficient (13 x 10^6 µm and 10^4-10^5 cm^{-1}, respectively). II-V semiconductors doped with transition metal ions like iron, nickel, and manganese are ideal candidates for dilute magnetic semiconductors (DMS), as their low carrier concentration and enhanced ferromagnetic exchange interactions between the magnetic ions make them particularly effective. In contrast to commonly researched transition metal (V, Cr, Mn, Fe) doped Zn_3P_2, a theoretical study was conducted based on ab initio [11]. Recent experimental investigations have investigated the optical, magnetic, and structural characteristics of Zn_3P_2 systems doped with several combinations of magnetic transition elements, including Mn, Ni, and Fe, as well as the paired combinations of Ni and Mn, Fe and Ni, and Fe and Mn [12-17].

In this study, we discuss a novel class of Zn_3P_2-based diluted magnetic semiconductors, explore various compounds from the II-V alloy family, and examine how these materials influence dopant behavior and magnetic properties.

2. Crystalline Structure of Zn_3P_2

D.M. Stepanchikov et al., [18] discussed the crystal structure and band structure of Zn_3P_2. Zn_3P_2 belongs to a family of four II-V semiconductors that share similar crystal structures, along with Cd_3P_2, Zn_3As_2, and Cd_3As_2. The variety of crystalline structures distinguishes substances with the chemical formula II-V from one another. Near the conventional FCC packing, they have anion surfaces. The tetrahedral vacuum is only partially filled by the cations of the anions. Due to the precise proportion of vacancies in their cation substrates, they may even be regarded as stoichiometric. All crystalline formations' distinctive properties are governed by various ways in which these vacancies are distributed. Examples of materials with a cubic symmetry include fully disordered high-temperature phosphide β-phases. Tetragonal symmetry is visible in the partially ordered crystals (α-phases).

T = 1118 K is the temperature at which Zn_3P_2 crystals undergo a phase transition (β→α). An energy of 0.078 eV is commonly associated with the positional order that results from this transition. In the following section, we aim to examine the low-temperature, moderately ordered tetragonal phases. The crystal structure of Zn_3P_2's tetragonal modification is characterized by a unit cell that has a primitive tetragonal lattice. Within this unit cell, there are a total of 16 phosphorus (P) atoms and 24 zinc (Zn) atoms, as seen in Figure 1. The space group assigned to the crystal structure is P42=nmc, and the unit cell parameters are determined to be a = b = 8.0889 and c = 11.4069.

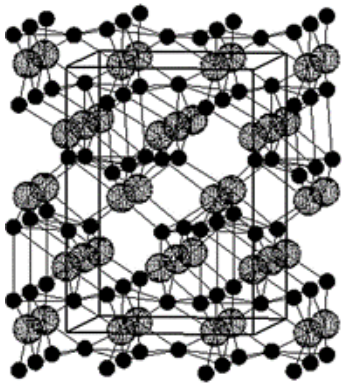

Figure 1. Typical representation of the Zn_3P_2 crystal structure, with larger spheres representing P and smaller spheres representing Zn atoms. Adapted from Ref. [18] Copyright 2009, Institute for Condensed Matter Physics.

The presence of vacancies in one-quarter of the cation sublattice positions enables differentiation between these crystalline structures. Although phosphorus atoms occupy only six of the eight corners of the cube, each zinc cation exhibits tetrahedral coordination with its four nearest phosphorus neighbors. The current scenario is characterized by the presence of these elements at just six out of the eight corners of the cube. On each of the diagonal corners of a cubic face, as well as at the opposite ends of the cubic diagonal, two vacant spaces may be seen. Figure 1 can be examined to see that there are four cations and two different types of phosphorus layers. The locations of cation vacancies vary between the four cation layers. This configuration, which consists of two stacked packets normal to the major axis, is considered by some writers to be the simplest polytype. The modified extended elementary cell, with dimensions of $a\sqrt{2}$ x $a\sqrt{2}$ x c, may be seen as the alternating arrangement of two distinct stacked packets along the primary axes X and Y. This is because the extended elementary cell has a larger surface area than the original elementary cell. Each packet consists of four atomic layers, which together form the extended elementary cell. Because the cations (A, C) and the anions (A, B) in the packet are positioned such that they are near one another, the equation X = A, B is true.

Furthermore, the use of the coordinate system of the extended elementary cell enables the transformation of packet X into packet Y, and vice versa, by the application of partial translations. These translations possess a value equivalent to $(a\sqrt{2} + c)/2$. This is accomplished via the use of partial translations. The principal axis of crystallography runs in a direction that is orthogonal to the atomic layers and the stacked packets. The contact between the metal atoms in such configurations, which are more tightly packed than in III-V and II-VI compounds, should be improved, increasing the metallic contribution to the chemical bond. These materials typically contain 4/3 electrons per bond, which is much less than the typical 2 electrons per bond seen in tetrahedral coordination semiconductors. This relative paucity of bonding electrons causes equilibrium bond lengths to shorten. A significant proportion of the link lengths within the tetrahedral coordination, namely 56 out of the total 96, exhibit proximity to or alignment with the sum of covalent radii, measuring 2.41 Å. Conversely, the remaining 40 bond lengths are seen to be shorter than the sum of ionic radii, which amounts to 2.86 Å. The coordinates corresponding to zero energy are found to be situated near the upper region of the hh-band. Based on this particular interpretation, it is suggested that the lh and hh valence bands exhibit the narrowest width.

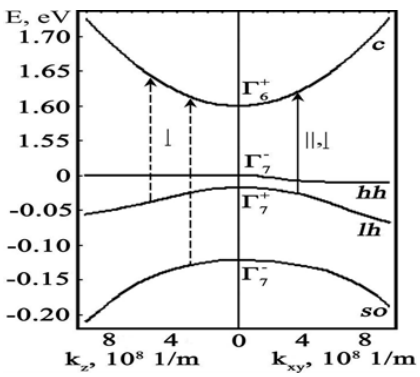

Figure 2. Zn_3P_2 Energy band structure. Adapted from Ref. [18] Copyright 2009, Institute for Condensed Matter Physics.

Figure 2 shows the energy band structure of Zn_3P_2. It is essential to comprehend selection principles to classify exciton states and to understand optical band-to-band transitions. The selection criteria for Zn_3P_2 are influenced by the light's polarization vector (ep). The highlighted transitions at the Γ point were those that were considered "allowed". These transitions included both the light polarised perpendicular (ep ⊥ c) and parallel (ep ∥ c) to the main crystallographic c-axis. Additionally, the transitions $\Gamma\pm \rightarrow \Gamma\mp$ were observed specifically for the light polarised perpendicular to the c-axis (ep ⊥ c; I, J 6.7). Figure 3 shows the allowed and forbidden transition of Zn_3P_2. Forbidden transitions in (ep ∥ c) are only seen when the value of k_0 is equal to zero. These transitions include the conversion of a state Γ± to a state Γ∓. These transitions are permitted close to the $k_0 = 0$ point. For the "allowed" transitions, only s-excitons can be produced, while only p-excitons can be produced for the "forbidden" transitions.

Both longitudinal and transverse excitations are produced under ($e_p \perp c$) polarization circumstances. However, in ($e_p \parallel c$) polarization circumstances, the longitudinal excitons are not produced. As is well known, stacked crystals have a higher likelihood of producing transversal excitons. As a result, only transverse excitons were taken into consideration hereunder.

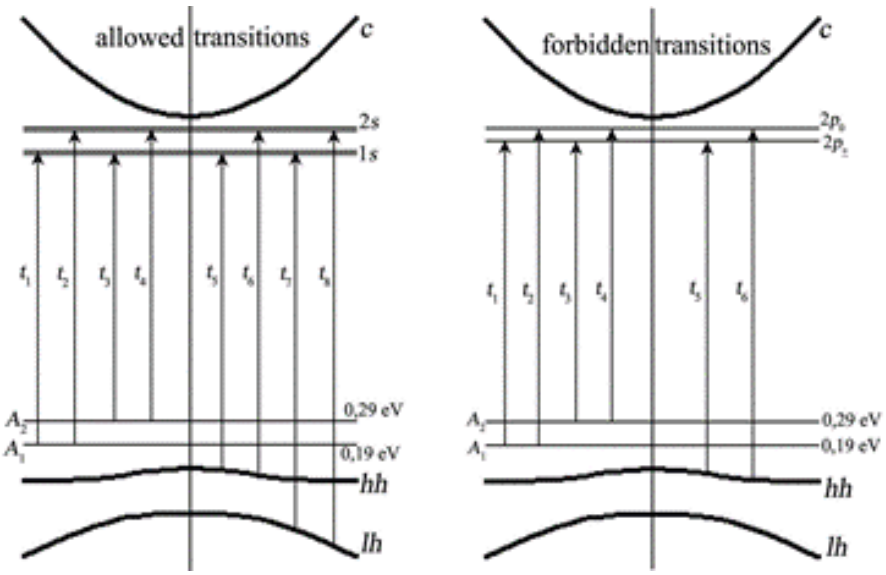

Figure 3. Diagrammatic representation of Zn_3P_2's localized level placements and transitions. Adapted from Ref. [18] Copyright 2009, Institute for Condensed Matter Physics.

The spin-orbit interaction was inadvertently omitted while calculating the exciton energy. Now, we have reached a stage where we may examine the two-exciton series, which exhibits coupling with the conduction band (c) as well as the valence bands associated with heavy and light holes (hh, lh). These assumptions have facilitated our progress up to this juncture. The permissible transitions of an exciton characterized by a principal quantum number of n=1 can elucidate a significant proportion of visual phenomena. The binding energy of the primary exciton state is either equivalent to or greater than the average thermal motion energy, which is about 25.8 meV when measured at room temperature and denoted as k_0T. This implies that the binding energy of the main exciton state is either equal to or greater than the average energy associated with thermal motion. Even under conditions of ambient temperature, it is possible to accurately forecast the specific wavelengths at which absorption or luminescence maxima occur in the optical spectrum. This may be attributed directly to the preceding discussion. This statement holds irrespective of the presence or absence of the 2D-exciton spectrum in bulk crystals or thin films, as well as its level of reinforcement. Furthermore, this is true irrespective of whether or not it has been reinforced.

3. Literature Survey of Zn_3P_2 and II-V Diluted Magnetic Semiconductors

3.1 II-V Group Diluted Magnetic Semiconductor

According to a literature survey of II-V group compounds, there is little work on room-temperature ferromagnetism. II-

group elements are Zn, Cd, Hg, Cn, and V- group elements are N, P, As, Sb, and Bi, combining these two groups form new compounds are Cd_3P_2, Cd_3As_2, $ZnAS_2$, Zn_3As_2, Zn_3P_2, etc. These dilute magnetic semiconductors are doped with transitional metal ions (Fe, Ni, Cr, and Co).

3.1.1 Fe-doped Zn_3P_2

To examine [19] the magnetic and electrical properties of Fe-doped zinc phosphide (Zn_3P_2), initial calculations were conducted using the density functional theory (DFT) as the foundational methodology. According to the findings of the experiment, both the ferromagnetic state and the half-metallic ground state are stable at low quantities of Fe. The heat of production was calculated, and the lowest total energies in the ferromagnetic and nonmagnetic phases were examined to determine the stability of the doped material. Calculations yield a significant value for the magnetic moment, and they imply that the Fe-doped Zn_3P_2 might be a viable material in semiconductor spintronics.

3.1.2 Ti-doped Zn_3P_2

The study used [20] first-principles density functional theory (DFT) calculations to examine the structural, electrical, and magnetic properties of the Ti-substituted Zn_3P_2 molecule. The study examines the effects of substituting one or two titanium (Ti) atoms in the Zn_3P_2 unit cell, which consists of eight molecules per formula unit and a total of 40 atoms. The findings of our study indicate that the substitution of a single Ti atom promotes the ferromagnetic phase due to its lower total energy compared to the nonmagnetic phase. Based on our calculations, it can be inferred that the magnetic moment at the titanium (Ti) location exhibits a significant magnitude.

3.1.3 Fe, Ti, V, Cr, Mn, Co doped Zn_3P_2

Using ab initio research, [11] studied a doped Zn_3P_2 matrix with transition elements (TM=Fe, Ti, Cr, Mn, and Co) and examined the magnetism, structural stability, and density of states that are spin-dependent as well as the half-metallic property. Transition metal atoms were inserted in the pure matrix at the concentrations of 2.5% and 5%. It has a stable ferromagnetic (antiferromagnetic) ground state and a half-metallic structure. The calculation of production heat was conducted to investigate the structural and magnetic stability of the substituted compounds. Specifically, the lowest total energies associated with the ferromagnetic, antiferromagnetic, and nonmagnetic phases were examined. Doped transition elements in a pure matrix are found to rise to the compounds' magnetism and the observed half-metallic property. Utilizing the charge density contours, researchers looked into this issue using the predicted densities of states for the atom, orbital, and spin. They also looked at the type of bonding in these systems. According to the computations, the magnetically stable phases exhibit significant magnetic mobility. Ultimately, these findings possess potential use in the realm of semiconductor spintronic applications. Additional X-ray diffraction findings were obtained, which were subsequently verified after the introduction of chromium doping into a pristine matrix. These results perfectly matched the pure matrix diffraction plane and all planes are very sharp and strong. It indicates the preferable crystallinity.

3.1.4 Fe, Ni, Mn, Ni-Mn, Fe-Ni and Mn-Fe doped Zn_3P_2

Recently discussed [12-17] the experimentally, aims specifically to attain room temperature ferromagnetism in Zn_3P_2 systems doped with transition metals and examine potential mechanisms for it. In the following sections, experiments and key observations of each dopant are briefed. In this study, iron, nickel, and manganese doped with zinc phosphide ($Zn_{3-x}TM_xP_2$), TM=Fe, Ni, Mn, Ni-Mn, Fe-Ni, and Mn-Fe) the system was synthesized by a solid-state reaction method. Structural, morphological, composition, optical, photoluminescence, and magnetic properties were investigated. The XRD analysis revealed that TM-doped samples showed a tetragonal structure and no secondary phase peaks were observed in the diffraction patterns.

The SEM study revealed that the size of agglomerations slightly increases with increasing dopant concentration. The elemental analysis confirmed that all the Fe, Ni, and Mn-doped Zn_3P_2 nanoparticles are nearly stoichiometric. The diffuse reflectance spectra were used to calculate the optical bandgap of the TM-doped Zn_3P_2 nanoparticles and it increased with the increase of dopant concentration. PL studies confirmed all emission peaks are in the same wavelength position and slight intensity changes with increasing dopant concentration. The M-H hysteresis loop of the pure and TM-doped Zn_3P_2 nanoparticles shows that the transition from weak to strong ferromagnetism correlates with increased dopant concentration, suggesting enhanced exchange interactions. The magnetic moment obtained from the present studies suggests that the TM-doped Zn_3P_2 nanoparticles may be a useful material in semiconductor spintronics. Table 1 shows the saturation magnetization of Zn_3P_2 doped with Fe, Ni, and Mn via solid-state reaction method.

Table 1. Transition metals (Fe, Ni, and Mn) doped Zn_3P_2 system, magnetization values based on experimental results

Sample	Magnetization (Ms) (emu/g)	References
$Zn_{0.92}Fe_{0.08}P_2$	0.2312	[12]
$Zn_{0.93}Ni_{0.07}P_2$	0.0418	[13]
$Zn_{0.92}Mn_{0.08}P_2$	0.1181	[14]
$Zn_{0.91}Ni_{0.02}Mn_{0.07}P_2$	0.2517	[15]
$Zn_{0.89}Fe_{0.02}Ni_{0.09}P_2$	0.2021	[16]
$Zn_{0.90}Mn_{0.02}Fe_{0.08}P_2$	0.2495	[17]

3.1.5 Ti-doped Cd_3P_2

In this investigation [21], the use of density functional theory is employed to analyze the magnetic and electrical properties shown by the Ti-doped Cd_3P_2 material. Pure Cd_3P_2 has a basic tetragonal form in its crystal structure at room temperature (space group: P42/nmc (137)). Eight units of the Cd_3P_2 formula, or 40 atoms (Cd=24 and P=16), are present in the unit cell. While the P atoms are located in the unit cell's 4c, 4d, and 8f P42/nmc symmetry sites, the Cd atoms occupy three different sorts of 8g places. The first and second Ti atoms are replaced by Cd_3P_2. According to the results of certain simulations, the magnetic moment of the Ti atom increased when it was substituted with the Cd atom. As a direct result of this, the system could exhibit magnetic order. According to the results, magnetic order is preferred in the system when it is in the ferromagnetic configuration. This configuration may be thought of as having one Ti atom swapped. This was shown by the fact that the system generated less total energy overall when compared to the simulations that did not consider spin polarisation. In the calculations for the ferromagnetic and antiferromagnetic configurations, the two Ti atoms that were located in the unit cell were switched out for other atoms. The evaluation of magnetic stability in the substituted compounds included the identification of the phase with the lowest total energy among the ferromagnetic, antiferromagnetic, and nonferromagnetic phases. This was done by comparing the energy levels of all three phases. Systems with one or two Ti atoms substituted in Cd_3P_2 exhibited features of metal and created magnetic order. These systems also exhibited metallic properties. According to the results of certain calculations, the magnetic moment of a titanium atom is rather big. The nearby cadmium and phosphorus atoms were found to contribute small magnetic moments.

3.1.6 Mn doped Zn_3As_2

This article examines, [22] the magnetic properties of $(Zn_{1-x}Mn_x)_3As_2$ with x = 0.08–0.13. To learn more about the existence and make sense of MnAs clusters in this material, samples with a rather high Mn content were used. It describes how various clusters affect the high-temperature magnetic freezing phenomenon. The modified Bridgman technique achieves the growth of ZMA single crystals, which involves the slow cooling of a molten substance in a furnace while subjecting it to a controlled temperature gradient. The discussion pertains to the structure, composition, and homogeneity of the specimens, as well as the details about their processing and characterization. The direct current (DC) magnetic measurements were conducted at two distinct temperature ranges: 3–310 K and 250–500 K. These measurements were performed using a SQUID magnetometer, which significantly expanded the temperature range from 5-220 K.

To eliminate any possible residual magnetism, the sample underwent an annealing procedure lasting between 0.5 and 2 hours at a temperature ranging from 150 to 200 °C before to each measurement. The investigation used a temperature range spanning from 3 to 500 K and magnetic fields of up to 60 kG to examine the magnetic properties of the $(Zn_{1-x}Mn_x)_3As_2$, an II-V diluted magnetic semiconductor. Upon increasing the temperature to 280 K, a notable reduction in the magnetization of all samples is seen. In the context of magnetic fields ranging from five to eighty G and temperatures below the blocking temperature of two hundred fifty degrees Kelvin, it can be shown that the temperature dependence of magnetic susceptibility exhibits mostly irreversible behavior. When the pressure exceeds 15 kG, the absence of zero field-cooled susceptibilities and field-cooled susceptibilities becomes apparent. There are likely two distinct magnetic subsystems that may be identified based on the existence of certain qualities. These properties include ferromagnetic MnAs nanoclusters as well as paramagnetic centers consisting of a single Mn ion and an antiferromagnetic cluster that can be either open or closed. Based on the results, it was observed that AF clusters larger than triplets had no discernible impact

on the PM response, up to a magnitude of 0.12 in the PM reaction. A phenomenon known as a blocking transition has been seen in the dynamics of the magnetic moments of the ferromagnetic (FM) clusters. This transition occurs at a temperature about ten percent lower than the Curie temperature associated with ferromagnetism in bulk MnAs. This discovery enabled the determination of the Curie temperature of ferromagnetism in bulk MnAs. The observed occurrences at low magnetic fields indicate an apparent irreversibility in the blocking transition, suggesting that it is irreversible. The observed size distribution of MnAs clusters in ZMA is found to be indistinguishable from that of $(Zn_{1-x}Mn_x)_3As_2$, suggesting that both materials undergo a comparable mechanism for generating MnAs nanoparticles.

3.1.7 Mn-doped $ZnAs_2$

The compound $Zn_{1-x}Mn_xAs_2$ may be synthesized by the process of replacing manganese (Mn) for zinc (Zn) in the compound $ZnAs_2$. The paper [23] provides an analysis of the attributes of the host material. The investigation focused on the synthesis of the $Zn_{1-x}Mn_xAs_2$ dilute magnetic semiconductor and its magnetic properties, to develop a novel series of II-V compounds including transition metal elements. Creating $Zn_{1-x}Mn_xAs_2$ single crystals requires a modified version of the Bridgman process. They have the same structure as the $ZnAs_2$ complex, which is their parent when x is 0. Between temperatures of 2 and 500 degrees Celsius, the magnetic properties of $Zn_{1-x}Mn_xAs_2$ are investigated at fields as high as 60 kG for x values of 0.01, 0.05, and 0.1. When temperatures are raised over 300 degrees Kelvin, the magnetic nature of every sample begins to rapidly drop. The magnetic susceptibility exhibits a high degree of irreversibility in response to temperature variations when subjected to low magnetic fields ranging from 2 to 200 G, particularly at temperatures below the critical temperature of around 250 K. This occurs when the temperature is low enough. After the magnetization has attained 100% saturation, a nonlinear field dependence may be seen between B~1-2 kG and 40 kG. This may be the case between the two values. Between 2 and 300 K, its reliance on temperature is almost non-existent. MnAs clusters are the key to deciphering the mystery behind the magnetic properties. The cluster size distribution that was generated makes use of three overlapping Gaussian functions, each of which reaches its maximum at 1.7, 2.4, and 3.3 nm. It is determined that the corresponding magnetic moments at 300 K are 1.5, 4.1, and 10.4 in terms of 10^3 μB.

3.1.8 Mn doped Cd_3As_2

In this study [24], investigated the properties of the semi-magnetic semiconductor $(Cd_{1-x}Mn_x)_3As_2$. Specifically, evaluated its magnetization, susceptibility, and specific heat across a temperature range spanning from 0.5 K to 300 K. Additionally, we explored these properties under the influence of magnetic fields up to 25 T, focusing on samples with a Mn concentration of 18%. The findings of these experiments had beneficial outcomes. The results of these tests have shown their reliability in producing accurate findings. A reduction in temperature may lead to an observed shift from the conventional glass state to the spin glass state. Based on the findings, it is evident that apart from the significantly influential closest neighbor interaction, there exists an antiferromagnetic (AF) long-range interaction, which may be characterized as either J_1/R^3 or J_1/R^4 in its nature. This phenomenon is seen at extended distances. The research findings indicate that the magnetic moment on the Mn sites is around 4.4 magnetons, and the distribution of magnetic ions is completely stochastic. To calculate the thermodynamic parameters, we used an extended iteration of the closest neighbor pair correlation technique, according to the provided specifications to direct our research efforts. The provided estimations of Cm, M, and X (Ki) seem to be reasonable, given the values of J_0/K_B= -30 K and J_1/K_B= -20/R^4 K (where R represents the distance to the nearest neighbor in units of Ki). In addition, we explore alternate hypotheses about the exchange mechanism in $(Cd_{1-x}Mn_x)_3As_2$ and examine the possible generalizability of our model to other semi-magnetic semiconductors.

3.1.9 Ti-doped Cd_3P_2

In this study [25], ab initio calculations were conducted using density functional theory to evaluate the magnetic and electrical properties of Cd_3P_2 compounds with one or two Ti atoms substituted. This was done to do the analysis. The nonmagnetic, ferromagnetic, and antiferromagnetic phases all had their lowest total energies studied so that the magnetic stability of the substituted compounds could be determined. According to the findings of our research, Cd_3P_2 complexes in which one or two Ti atoms were substituted may have developed magnetic order and metallic properties. The Ti atom should have a substantial magnetic moment, according to our hypothesis. Furthermore, it has been shown that the proximity of Cd and P atoms leads to the generation of a minor magnetic moment.

Table 2. Literature survey of Zn_3P_2

System	Form	Technique followed	Observations	References
Experimental				
Blulk				
Zn_3P_2	Crystal	Vapor transport using a Capsule method	The capsule method is used to control the vapor composition during the vapor growth process.	[26]
Zn_3P_2, Cd_3P_2, Cd_3As_2	Crystal	Static sublimation and Piper-Polich	Periodic bond chain (PBC) analysis	[27]
Zn_3P_2	Crystal	-	Chemical bonding from X-ray diffraction analysis and deformation density maps	[28]
Zn_3P_2: In	Crystal	Flux technique	Growth of bulk crystals and Hall effect measurement analysis	[29]
Zn_3P_2: Li	Crystal	Ball milling	Structural and ion batteries analysis	[30]
Thin films				
Zn_3P_2	Thin film	Physicochemical method	Study of optical properties of nanocrystalline materials, X-diffraction, and surface morphology	[31]
Zn_3P_2	Thin films	Plasma-assisted vapor phase deposition (PAVPD)	Electrical and optical properties using substrate temperature	[32]
Zn_3P_2	Thin films	Co-Evaporation	Structural, morphological, and optical properties studies	[33]
Zn_3P_2	Thin films	Hot-wall deposition	Growth rate, structural and electrical properties	[34]
Zn_3P_2	Thin films	Metalorganic chemical vapor deposition (MOCVD)	x-ray diffraction and electrical conductivity analysis of growth temperature	[35]
Zn_3P_2	Thin films	Hot wall deposition	Optical absorption and photoconductivity studies	[36]
Zn_3P_2	Thin films	Tauc power Law	Energy gap based on temperature dependences	[37]
Zn_3P_2 and Cd_3P_2	Thin films	Metalorganic chemical vapor deposition (MOCVD)	x-ray diffraction, photoluminescence, photoconductivity, and Hall effect studies	[38]
Zn_3P_2 and Cd_3P_2 alloy	Thin films	Electron beam evaporation	Electrical conductivity, Photoconductivity, and Hall mobility analysis	[39]
Zn_3P_2	Thin films	Close space evaporation	Source to substrate distance	[40]
Zn_3P_2	Thin films	Vacuum deposition	Low-energy electron bombardment	[41]
Zn_3P_2	Thin films	Hot wall deposition	Low resistivity	[42]
Theoretical				
Zn_3P_2	DFT-LCAO (Linear combinations of atomic orbital method) calculations		Structural and Electrical Properties Using the LCAO method finds the electronic structure calculations	[43]
Zn_3P_2	Pseudopotential		Band structure and properties of Zn_3P_2	[44]
Zn_3P_2	Density functional theory (DFT)		Zinc phosphide nanowires for photochemical H2 production	[45]

Table 2 shows the literature survey of Zn_3P_2 and its observations. Table 2 describes the Zn_3P_2 system's many qualities, including its structural, optical, electrical, and magnetic characteristics, and how it is employed in various deposition processes. Furthermore, thin-film production of the Zn_3P_2 system with doping transition and rare earth elements is feasible in the future. The Zn_3P_2 semiconductor thin films had emerged as promising solar cell materials. One of the major advantages of this material is that it is available in sufficient abundance to fulfill the requirements of large-scale power generation.

4. Conclusion

In summary, Zn_3P_2 is an abundant and cost-effective material naturally found on Earth. According to the current and previous literature review, there has been less research done on this topic than on other diluted magnetic semiconductors (II-IV, IV-VI, and II-VI). The majority of academics invited theoretical studies for spintronic applications in the Zn_3P_2 system. The Zn_3P_2 system's ferromagnetism was verified by theoretical and experimental investigations using transition elements (V, Cr, Mn, Fe, and Co). Furthermore, the Zn_3P_2 system may be susceptible to ferromagnetism if doped with rare-earth metals. Zn_3P_2 is an experimentally studied semiconducting material that will be employed in spintronic applications and lithium-ion batteries in the future. Zn_3P_2 may also be easily deposited in thin films utilizing chemical and physical deposition methods, and it is utilized in optoelectronic applications. Additionally, we comprehended the Zn_3P_2 system applied to the manufacturing of solar cell devices. We believe this material holds great promise for human society since it can be used in a greater number of low-cost applications.

Acknowledgment

The authors would like to thank Nasina Madhusudhana Rao for his valuable suggestions.

Funding

No funding, grants, or other assistance were obtained to prepare this work.

Data Availability

Data supporting this study's conclusions are accessible from the corresponding author upon reasonable request.

Declarations

Conflict of interest: Authors declare no conflict of interest in this study.

Ethical Approval

This article does not include any experiments conducted by the authors using human participants or animals. In this investigation, no human or animal samples were collected.

References

[1] Dietl T. A ten-year perspective on dilute magnetic semiconductors and oxides. Nat Mater. 2010;9:965-74. doi:10.1038/nmat2898.

[2] Dietl T. Origin of ferromagnetic response in diluted magnetic semiconductors and oxides. J Phys Condens Matter. 2007;19:165204. doi:10.1088/0953-8984/19/16/165204.

[3] Dietl T, Ohno H. Dilute ferromagnetic semiconductors: Physics and spintronic structures. Rev Mod Phys. 2014;86:187-251. doi:10.1103/RevModPhys.86.187.

[4] Dietl T. Origin of ferromagnetic response in diluted magnetic semiconductors and oxides. J Phys Condens Matter. 2007;19:165204. doi:10.1088/0953-8984/19/16/165204.

[5] Sathyamoorthy R, Sharmila C, Natarajan K, Velumani S. Influence of annealing on structural and optical properties of Zn3P2 thin films. Mater Charact. 2007;58:745-9. doi:10.1016/j.matchar.2006.11.015.

[6] Soliman M, Kashyout AB, Osman M, El-Gamal M. Electrochemical deposition of Zn3P2 thin film semiconductors on tin oxide substrates. Renew Energy. 2005;30:1819-29. doi:10.1016/j.renene.2005.01.004.

[7] Nayak A, Banerjee HD. X-ray photoelectron spectra of Zn3P2-Cd3P2 alloy semiconducting thin films. Mater Chem Phys. 1999;60:95-8. doi:10.1016/S0254-0584(99)00064-4.

[8] El Zawawi IK, Moez AA, Hammad TR, Ibrahim RS. Phase transformation and disorder effect on optical and electrical properties of Zn3P2 thin films. Spectrochim Acta A Mol Biomol Spectrosc. 2012;94:378-83. doi:10.1016/j.saa.2012.03.072.

[9] Bhushan M, Turner JA, Parkinson BA. Photoelectrochemical investigation of Zn3P2. J Electrochem Soc. 1986;133:536. doi:10.1149/1.2108615.

[10] Villars P, Calvert LD. Pearson's handbook of crystallographic data for intermediate phases. American Society of Metals; 1985.

doi:10.1557/S0883769400069682.

[11] Jaiganesh G, Jaya SM. Magnetism, electronic structure and half-metallic property of transition metal (V, Cr, Mn, Fe, Co) substituted Zn3P2 dilute magnetic semiconductors: an ab-initio study. Comput Mater Sci. 2015;102:85-94. doi:10.1016/j.commatsci.2015.02.018.

[12] Praveenkumar N, Rao NM. Room temperature ferromagnetism in undoped and Fe doped Zn3P2 nanoparticles: Structural, optical and magnetic properties. Solid State Sci. 2024;151:107519. doi:10.1016/j.solidstatesciences.2024.107519.

[13] Praveenkumar N, Rao NM. Ni doped Zn3P2 nanoparticles: Synthesis, structural, optical, and magnetic properties. J Supercond Nov Magn. 2023;37:1-13. doi:10.1007/s10948-023-06670-w.

[14] Praveenkumar N, Rao NM, Chakravarthi MK. Structural, optical, and magnetic properties of Mn doped Zn3P2 diluted magnetic semiconductor nanoparticles. ECS J Solid State Sci Technol. 2024;13:054003. doi:10.1149/2162-8777/ad47d1.

[15] Praveenkumar N, Rao NM. Transition metal (Ni, Mn) codoped Zn3P2 nanoparticles: effect on structural, optical and magnetic properties. Nano Express. 2023;4:045009. doi:10.1088/2632-959X/ad0e78.

[16] Praveenkumar N, Rao NM. The effect of Fe and Ni dual-doping on the structural, optical and magnetic properties of Zn3P2 nanoparticles. Appl Phys A. 2024;130:271. doi:10.1007/s00339-024-07413-x.

[17] Praveenkumar N, Rao NM. Synthesis of (Mn, Fe) co-doped Zn3P2 nanoparticles: structural, optical and magnetic properties via solid-state reaction route. J Mater Sci Mater Electron. 2024;35:719. doi:10.1007/s10854-024-12512-9.

[18] Stepanchikov DM, Chuiko GP. Excitons into one-axis crystals of zinc phosphide (Zn3P2). Condens Matter Phys. 2009;12:239. doi:10.5488/CMP.12.2.239.

[19] Jaiganesh G, Jaya SM. Half-metallic ferromagnetism in Fe-doped Zn3P2 from first principles calculations. AIP Conf Proc. 2014;1591:1081-3. doi:10.1063/1.4872860.

[20] Sekaran JG, Jaya SM. Effect of partial Ti substitution at Zn sites on the structural, electronic and magnetic properties of Zn3P2. Authorea Preprints. 2020. doi:10.22541/au.160466779.91279508/v1.

[21] Jaiganesh G, Jaya SM. Electronic structure and magnetism of titanium substituted Cd3P2 an ab-initio study. AIP Conf Proc. 2018;1953:030017. doi:10.1063/1.5033127.

[22] Laiho R, Lisunov KG, Lahderanta E, Zakhvalinskii VS. Magnetic MnAs nanoclusters in the diluted magnetic semiconductor (Zn1-xMnx)3As2. J Phys Condens Matter. 1999;11:8697. doi:10.1088/0953-8984/11/44/310.

[23] Laiho R, Lisunov E, Lähderanta V, Zakhvalinskii S. Magnetic properties of the new diluted magnetic semiconductor: evidence of MnAs clusters. J Phys Condens Matter. 1999;11:555. doi:10.1088/0953-8984/11/2/018.

[24] Denissen CJM, Nishihara HV, De Gool JC, Jonge WJM. Magnetic behaviour of the semi magnetic semiconductor (Cd1−xMnx)3As2. Phys Rev B. 1986;33:7637. doi:10.1103/PhysRevB.33.7637.

[25] Jaiganesh G, Jaya SM. Electronic structure and magnetism of titanium substituted Cd3P2 an ab-initio study. AIP Conf Proc. 2018;1953:030017. doi:10.1063/1.5033127.

[26] Catalano A. The growth of large Zn3P2 crystals by vapour transport. J Cryst Growth. 1980;49:681-6. doi:10.1016/0022-0248(80)90294-8.

[27] Kloc K, Żdanowicz W. Growth and morphology of Zn3P2, Cd3P2 and Cd3As2 crystals. J Cryst Growth. 1984;66:451-8. doi:10.1016/0022-0248(84)90229-X.

[28] Zanin IE, Aleinikova KB, Afanasiev MM, Antipin MY. Structure of Zn3P2. J Struct Chem. 2004;45:844-8. doi:10.1007/s10947-005-0067-9.

[29] Katsube R, Hayashi H, Nagaoka A, Yoshino K, Nose Y, Shirai Y. Growth and characterization of indium-doped Zn3P2 bulk crystals. Jpn J Appl Phys. 2016;55:041201. doi:10.7567/JJAP.55.041201.

[30] Li X, et al. Self-supported Zn3P2 nanowires-assembly bundles grafted on Ti foil as an advanced integrated electrodes for lithium/sodium ion batteries with high performances. J Alloys Compd. 2017;724:932-9. doi:10.1016/j.jallcom.2017.07.016.

[31] Bouzara C, Kaci S, Boukezzata A, Kezzoula F, Bozetine I, Keffous A, Ouadah Y. Study of optical properties of nanocrystalline zinc phosphide thin films. Silicon. 2019;11:331-7. doi:10.1007/s12633-018-9866-4.

[32] Suda T. Zinc phosphide thin films grown by plasma assisted vapour phase deposition. J Cryst Growth. 1990;99:625-9. doi:10.1016/0022-0248(90)90596-D.

[33] Lousa A, Bertran E, Varela M, Morenza JL. Deposition of Zn3P2 thin films by evaporation. Sol Energy Mater. 1985;12:51-6. doi:10.1016/0165-1633(85)90023-1.

[34] Fuke S, Imai T, Kawasaki K, Kuwahara K. Substrate effect on the deposition of Zn3P2 thin films prepared by a hot-wall method. J Appl Phys. 1989;65:564-6. doi:10.1063/1.343142.

[35] Kakishita K, Baba T, Suda T. Zn3P2 thin films grown on glass substrates by MOCVD. Thin Solid Films. 1998;334:25-9. doi:10.1016/S0040-6090(98)01110-9.

[36] Babu V, Suresh PR, Vaya P, Sobhanadri J. Electrical and thermoelectrically properties of Zn3P2 films grown by the hot wall epitaxy technique. J Appl Phys. 1988;64:1922-6. doi:10.1063/1.341744.

[37] Bryja L, Jezierski K, Ciorga M, Bohdziewicz A, Misiewicz J. Temperature dependence of energy gap of amorphous thin films of Zn3P2. Vacuum. 1998;50:5-7. doi:10.1063/1.341744.

[38] Hermann AM, Madan A, Wanlass MW, Badri V, Ahrenkiel R, Morrison S, Gonzalez C. MOCVD growth and properties of Zn3P2 and Cd3P2 films for thermal photovoltaic applications. Sol Energy Mater Sol Cells. 2004;82:241-52. doi:10.1016/j.solmat.2004.01.021.

[39] Nayak A, Rao DR. Electrical properties of electron-beam-evaporated Zn3P2 and Cd3P2 alloy films. Mater Chem Phys. 1994;37:225-9. doi:10.1016/0254-0584(94)90157-0.

[40] Murali KR. Thickness dependence of dc conductivity of amorphous Zn3P2 films. J Mater Sci Lett. 1986;5:418-20. doi:10.1007/BF01672347.

[41] Sacken U, Brodie DE. Effects of electron bombardment during vacuum deposition of Zn3P2 films. Can J Phys. 1985;63:757-61.

[42] Haque A, Brodie DE. The preparation and some properties of low resistivity Zn3P2 films prepared using a hot-wall deposition method. Can J Phys. 1989;67:893-5.

[43] Kaur M, et al. Investigation of structural and electronic properties of Zn3P2: Theory and experiment. J Electron Mater. 2016;45:2847-54. doi:10.1007/s11664-016-4455-z.

[44] Pawlikowski JM. Comments on Zn3P2 band structure. J Appl Phys. 1982;53:3639-42. doi:10.1063/1.331146.

[45] Ramos-Sanchez G, et al. Organic molecule-functionalized Zn3P2 nanowires for photochemical H2 production: DFT and experimental analyses. Int J Hydrogen Energy. 2014;39:19887-98. doi:10.1016/j.ijhydene.2014.10.028.